Laser-induced breakdown of an optically trapped gold nanoparticle for single cell transfection

Yoshihiko Arita,[1],* Martin Ploschner,[1] Maciej Antkowiak,[1,2] Frank Gunn-Moore,[2] and Kishan Dholakia[1]

[1]*SUPA, School of Physics and Astronomy, University of St Andrews, St Andrews, Fife KY16 9SS, UK*

[2]*SULSA, School of Biology, Medical and Biological Sciences Building, University of St Andrews, St Andrews, Fife KY16 9TF, UK*

Corresponding author: ya10@st-andrews.ac.uk

The cell selective introduction of therapeutic agents remains a challenging problem. Here we demonstrate spatially controlled cavitation instigated by laser-induced breakdown of an optically trapped single gold nanoparticle of diameter 100 nm. The energy breakdown threshold of the gold nanoparticle with a single nanosecond laser pulse at 532 nm is three orders of magnitude lower than water, which leads to nanocavitation allowing single cell transfection. We quantify the shear stress to cells from the expanding bubble and optimize the pressure to be in the range of 1–10 kPa for transfection. The method shows transfection of plasmid DNA into individual mammalian cells with an efficiency of 75%.   © 2013 Optical Society of America

OCIS codes: (140.3440) Laser-induced breakdown; (140.7010) Laser trapping; (170.7170) Ultrasound; (240.6680) Surface plasmons.

http://dx.doi.org/10.1364/OL.38.003402

The transfection of genes and injection of therapeutic agents into individual mammalian cells are among the most important research tools in modern molecular biology [1]. The use of acoustic bubbles in the proximity of cells oscillated by ultrasonic irradiation (insonation) can lead to enhanced membrane permeabilization of cells, and is known as sonoporation. Acoustic streaming, shock waves, and liquid microjets associated with the dynamics of cavitation bubble are implicated in gene and drug delivery into cells [2]. This approach, however, often leads to nonuniform and sporadic molecular uptake that lacks cell selectivity and suffers from a significant loss of cell viability.

Recently a suite of optical methods in the domain of cavitation-based therapies has provided the potential of sterility, reconfigurability, and single cell selectivity [3]. Laser-induced breakdown (LIB) of a liquid medium containing cells, has demonstrated cell lysis, necrosis or membrane permeabilization, with the outcome dependent upon the hydrodynamic shear stress to cells caused by the expanding bubble [4]. However, the relatively high energy deposition required for this process resulted in a much larger cavitation bubble (typically >200 μm in diameter) compared to the typical cell size that effectively reduces cell viability and has been detrimental to allow its wider usage.

More spatially controlled cavitation may be achieved by optically trapping particles for subsequent LIB instead of the surrounding liquid [5]. Optical tweezers allow the positioning of individual nanoparticles or microparticles at a desired location within the buffer medium. Therefore, using this tool for LIB offers additional degrees of freedom—the particle material, its size, and the LIB position relative to cells or tissues. We have shown that the LIB of trapped polystyrene nanoparticles significantly reduced the energy required for cavitation [6,7]. This leads to the permeabilization of cell membranes and transfection of cells in a targeted area in the absence of a lysis zone of cells.

Gold nanoparticle clusters have played a key role in this field, through antibody binding and sequestration with subsequent irradiation by nanosecond or femtosecond laser pulses [8–10]. A unique interaction of gold nanoparticles with light, known as surface plasmon resonance, can lead to strong absorption of light for heat generation. However, the introduction of gold nanoparticles in the cellular environment requires conjugation to the cells of interest and so nonspecific binding can occur. Furthermore, in many cases it is advantageous to obtain single cell spatial selectivity and to perform cell transfection in a label-free manner and not interfere with a cell in its native state. Recently, a photothermal nanoblade, which utilizes a Ti-coated glass microcapillary tip located in close proximity to the cell membrane, in tandem with nanosecond laser pulses, was demonstrated for cell membrane poration [11,12]. However, this approach requires a mechanical probe. An optical "noncontact" technique that provides single highly controlled nanobubble generation, adjacent to individual cells for transfection, would be highly advantageous in this field.

In this Letter, we demonstrate LIB of a gold nanoparticle where the energy deposition required for cavitation is three orders of magnitude lower than the breakdown threshold for water. Manipulation of the nanoparticle position relative to the cell membrane allows exceptional spatial control and targeting of single cells at will for transfection. We model the temperature rise >10^6 K due to heat generation when the trapped gold nanoparticle is irradiated with a single nanosecond laser pulse with a wavelength near the plasmon resonance frequency. We explore the dynamics of the cavitation bubble caused by this localized heat absorption, based on the nanosecond time-resolved images of cavitation. This allows us to quantify the hydrodynamic shear stress created by the expanding bubble at different radial positions, at different times. We demonstrate transfection of plasmid DNA into CHO-K1 cells with an efficiency of 75% by optimizing the shear stress on cells, i.e., optimizing the

relative position between the cell and nanoparticle (and thus nanobubble), without any loss of cell viability.

A single gold nanoparticle (100 nm in diameter) was trapped by a 1070 nm continuous wave (CW) fiber laser (IPG Laser GmbH, YLM-5-1070-LP: power of 80 mW). A single pulse of 532 nm frequency-doubled Q-switched Nd: YAG laser (Elforlight Ltd., SPOT: pulse width of 1 ns, energy of 10 nJ) was used to effect LIB of the trapped gold nanoparticle. Both of the beams were coaligned and focused by the same microscope objective (Nikon Ltd., E plan 100×, NA = 1.25 in oil) at a predefined axial location of 10 μm above the substrate, but within the cell culture medium. Quadrant photodiodes were used to monitor the scattered light from the trapped particle to ensure it was solely a single gold nanoparticle that was held in the trap.

A second 532 nm Nd:YAG laser (Elforlight Ltd., SPOT: pulse width of 1 ns) was used for illumination, which delivers a single nanosecond pulse at a desired time delay after the LIB event. Both the nanosecond lasers (one for LIB and the other for illumination) were triggered at a desired timing using a digital delay generator (Stanford Research Systems Inc., DG645, time resolution of 5 ps). Images of the LIB events, at time delays between the laser pulses of 0–500 ns, were recorded by a CCD camera (Imaging Source, DMK31BU03) triggered synchronously with the nanosecond lasers. As a result, one stroboscopic image was captured for each triggered LIB event.

The gold nanoparticles (BBI solutions, EMGC100) were suspended in Opti-MEM (Invitrogen Ltd.), containing plasmid DNA (encoding Mito-DsRed; Clontech) of 10 μgm ℓ^{-1}, to yield a concentration of ~10^6 mℓ^{-1}. CHO-K1 cells cultured on a glass-bottomed dish (WPI Ltd., 35 mm) with a confluency of $\lesssim$50% were prepared in this stock suspension. Ten individual gold nanoparticles per sample, were carefully positioned at the axial location of 10 μm from the substrate and at the radial positions of either <5, 10, or 50 μm from the center of cell nucleus. After 10 LIB events, the stock suspension was replaced with cell culture medium, Dulbecco's Modified Eagle's Medium (DMEM, Sigma-Aldrich Co. Ltd.) with 10% fetal calf serum (FCS, Globepharm Ltd.), 20 μgm ℓ^{-1} streptomycin (Sigma-Aldrich Co. Ltd.) and 20 μgm ℓ^{-1} penicillin (Sigma-Aldrich Co. Ltd.). The cells were incubated at 37°C with 5% CO_2 for 48 h to express the gene of interest. A minimum of five samples ($N = 5$) were treated for each radial position in the same manner to obtain reliable statistics.

We first modeled the amount of energy absorbed by the gold nanoparticle positioned at the focus of the beam (532 nm) using the COMSOL Multiphysics software (RF module in scattering formulation). The incoming beam was considered as a paraxial Gaussian beam in the far-field expression $\mathbf{E}_\infty$ of the angular spectrum decomposition, which is a valid approximation when the beam diameter is large (5 mm) in the back-focal plane of the objective [13]. We subsequently discretized the far-field reference sphere into 12 intervals in polar angle (0…70°), where the maximum polar angle is given by the maximum achievable angle for the objective with NA = 1.25 with the interface of glass ($n_g = 1.518$) and water ($n_w = 1.33$), and 30 intervals in azimuthal angle (0…360°). This allowed us to model the inside of the

far-field reference sphere with the refractive index of water ($n_w = 1.33$) while the outside of the sphere has the index of air ($n_a = 1$). The focal field using these assumptions, which neglect the change in the angular spectrum due to the presence of the glass–water interface, is subsequently utilized for comparison of the power flow in the computational domain either with or without a gold nanoparticle positioned at the highest intensity region of the focal field. This comparison revealed that approximately 38% of the injected power is absorbed by the gold nanoparticle. This amount of absorption is in line with other work on heating of trapped gold nanoparticles, which uses the same approximations we make [14]. For a single 1 ns laser pulse, of energy 10 nJ, the heat transfer model shows that the absorbed energy is strongly localized in the close proximity of the gold nanoparticle at the end of the pulse [Fig. 1(a)]. The dissipation of the heat through conduction into water is negligible due to poor thermal conductivity of water in this time scale. The deposited energy is able to raise the temperature of the gold nanoparticle by a million Kelvin [Fig. 1(b)] at the end of the 1 ns pulse. This calculated temperature indicates an upper limit as we neglect the vaporization of water and the phase change of gold. Optical breakdown can take place, leading to the formation of plasma and emission of shockwaves by its expansion followed by the vaporization of the nanoparticle or liquid (surrounding aqueous medium) [15].

Figure 2 shows a series of time-resolved images of the expansion and collapse of the cavitation bubble initiated at an axial position, Z_0 of 10 μm from the substrate. The maximum bubble radius, R_{max}, reached ~3 μm at ~150 ns, which is typically two orders of magnitude smaller than that of the LIB of a liquid alone. A stand-off parameter, $\gamma > 3$ ($= Z_0/R_{max}$) suggests that a jet flow formed toward the nearby substrate during the collapse phase had a minor effect on the experimental outcomes we observed.

The temporal evolution of the radial position, $R_B(t)$, of the bubble wall is shown in Fig. 3(a). A minimum of 10 images were used to obtain the average and standard deviation (2σ) at each data point shown. The bubble wall velocity, $V_B(t) = (dR_B(t)/dt)$, is shown in Fig. 3(b). The transient external fluid velocity, $V_\infty(r, t)$, produced by the cavitation bubble expansion was determined by applying the conservation of mass for an incompressible fluid in spherical coordinates:
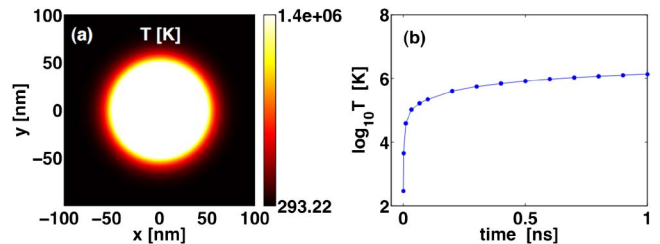

Fig. 1.   (a) Temperature profile in the vicinity of gold nanoparticle at the end of 1 ns pulse. The absorbed energy from the pulse was modeled as a uniform heat source within the volume of the nanoparticle. (b) Calculated temperature at the surface of the nanoparticle. This increases dramatically in the duration of the pulse.
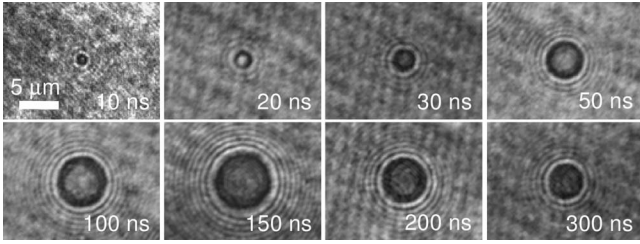
Fig. 2.   Time-resolved images of cavitation bubbles at time delays between 10 and 300 ns after the LIB event.

$$V_\infty(r, t) = V_B(t)\left[\frac{R_B(t)}{r}\right]^2. \qquad (1)$$

Conservation of momentum was then applied to obtain the transient wall shear stress $\tau_w(r, t)$:

$$\tau_w(r, t) = \rho\sqrt{\frac{\nu}{\pi}}\int_0^t \frac{\partial V_\infty(r, t')}{\partial t'}\frac{dt'}{\sqrt{t - t'}}, \qquad (2)$$

where $\rho(= 1000\ \mathrm{kgm^{-3}})$ and $\nu(= 0.896 \times 10^{-6}\ \mathrm{m^2\,s^{-1}})$ are the density of the liquid and kinematic viscosity of the buffer medium [4,6]. Equation (2) is valid at any radial position r and time $0 < t < t'$, where t' is the time of arrival of the bubble wall at position r. The temporal profile of the wall shear stress at different radial positions is shown in Fig. 3(c). The model revealed that the maximum shear stress decreases with increasing radial position, as shown in Fig. 3(d), and is <1 kPa only at $r = 15$ μm, which is typically three orders of magnitude lower than LIB in water alone [4].

Previously, we quantified that an applied shear stress to CHO-K1 cells of more than 10 kPa, causes cell necrosis, while between 1 and 10 kPa, enhances the membrane permeability without any loss of cell viability [6]. Cells located at radial positions between 5 and 13 μm from the site of the LIB of a gold nanoparticle [the shaded region in Fig. 3(d)], fall into the latter category. We investigated transfection of Mito-DsRed encoding plasmids into CHO-K1 cells at different radial positions.
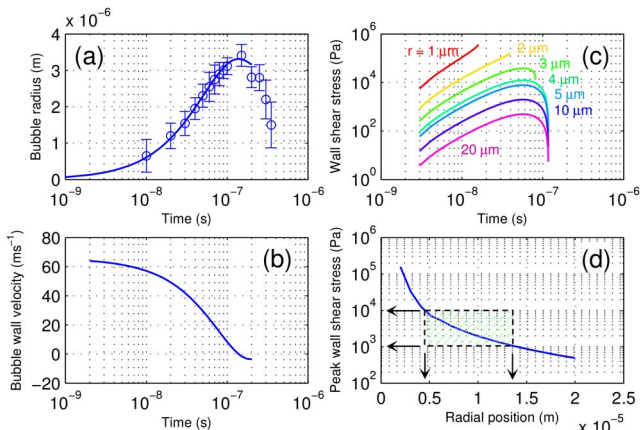

Fig. 3.   Cavitation bubble dynamics and wall shear stress. (a) Evolution of bubble radius, $R_B(t)$. (b) Bubble wall velocity, $V_B(t)$. (c) Temporal shear stress at radial positions, $\tau_w(r, t)$. (d) Maximum shear stress at radial positions, $\tau_{w,\max}(r)$.
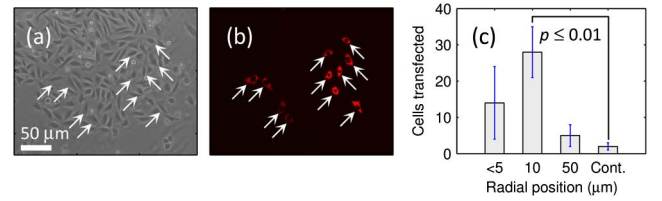

Fig. 4.   Transfection of Mito-DsRed encoding plasmids into CHO-K1 cells. (a) Phase contrast image of cells in the region of interest. (b) Fluorescence image of (a) showing 11 cells transfected (indicated by arrows). (c) Number of cells transfected with different radial positions (48 h after LIB). The error bars show two standard deviations. P value of ≤ 0.01 is a result from the unpaired t-test between $r = 10$ μm and control ($N = 5$ each).

Figure 4(a) shows a phase contrast image of cells and Fig. 4(b) the corresponding fluorescence image of the region of interest (48 h after LIB) showing 11 cells transfected. The number of cells transfected with different radial positions is shown in Fig. 4(c).

Cells at the radial position of 10 μm receive the maximum shear stress of ~2 kPa, which is optimum for cell membrane permeabilization. The number of cells transfected was typically ~30 (48 h after the treatment) for 10 treated cells per sample at $r = 10$ μm. We obtain the *corrected* transfection efficiency of ~75% as (30 transfected cells) divided by ($10 \times 2^{n=2} = 40$ treated cells) by assuming cells to divide twice ($n = 2$) in the subsequent 48 h [16,17]. When the cavitation occurs too close to the cell membrane ($r < 5$ μm), the shear stress exceeds 10 kPa and the bubble tends to collapse asymmetrically, often forming high speed liquid jets directed toward the cell membrane, which effectively reduces cell viability [6]. The control cells were exposed to the CW and nanosecond lasers, with gold nanoparticles in the buffer medium, but without any trapped particle, i.e., no LIB.

The cell membrane dynamics of permeabilization is not well understood at a molecular level. However, the transient shear stress causes cell lysis, necrosis, and membrane permeabilization depending on pressure [4,6,18,19]. In contrast to sonoporation, which lacks spatial confinement, LIB is an excellent tool for localized cavitation that allows us to treat a selective zone of cells. LIB of optically trapped microparticles and nanoparticles provided additional degrees of freedom in the domain of laser-induced cavitation. The energy deposition required for LIB is dependent on the trapped particle material and its size. Table 1 compares the photomechanical transduction process in LIB for water, polystyrene, and gold

Table 1.   Photomechanical Transduction Process in LIB for Water, Polystyrene (PS) 400 nm, and Gold (Au) 100 nm[a]

	E_p [μJ]	$R_{\max}$ [μm]	E_B [nJ]	E_B/E_p [%]	$\tau_{w,\max}$ [kPa]
Water [4]	8	118	340	4.3	1000
PS, 400 nm [6]	0.58	35	8.8	1.5	300
Au, 100 nm	0.01	3	0.011	0.11	2

[a]Laser pulse energy E_p, maximum bubble radius $R_{\max}$, mechanical bubble energy E_B, mechanical transduction efficiency E_B/E_p, and maximum wall shear stress at $r = 10$ μm.

nanoparticles, respectively, where the energy of a spherical bubble, E_B, is given by

$$E_B = \frac{4}{3}\pi(p_\infty - p_v)R_{\max}^3, \qquad (3)$$

where p_∞ is the static pressure of the surrounding liquid and p_v is the vapor pressure of the liquid (2330 Pa at 293 K) [20]. Remarkably, the energy deposition, E_P, required for the LIB of gold nanoparticles is three orders of magnitude less than that of water. Optical trapping for LIB allows exquisite control of the nanobubble energy, E_B, from >300 nJ (for water) down to 0.01 nJ (for gold) ranging over four orders of magnitude. The resultant pressure from the cavitation event can be optimized for transfection or delivery of molecules of interest, into a selective zone of cells/tissues or individual cells using this technique of LIB of optically trapped nanoparticles.

In summary, LIB of an optically trapped gold nanoparticle significantly reduces the energy required for cavitation, enabling the single cell transfection and delivery of molecules. This methodology and approach present a significant step forward in the application of optically controlled cell selective transfection.

References

1. D. J. Stevenson, F. J. Gunn-Moore, P. Campbell, and K. Dholakia, J. R. Soc. Interface **7**, 863 (2010).
2. S. Mitragotri, Nat. Rev. Drug Discovery **4**, 255 (2005).
3. K. R. Rau, A. Guerra, A. Vogel, and V. Venugopalan, Appl. Phys. Lett. **84**, 2940 (2004).
4. K. R. Rau, P. A. Quinto-Su, A. N. Hellman, and V. Venugopalan, Biophys. J. **91**, 317 (2006).
5. Y. Arita, M. L. Torres-Mapa, W. M. Lee, T. Cizmar, P. Campbell, F. J. Gunn-Moore, and K. Dholakia, Appl. Phys. Lett. **98**, 093702 (2011).
6. Y. Arita, M. Antkowiak, V. Venugopalan, F. J. Gunn-Moore, and K. Dholakia, Phys. Rev. E **85**, 016319 (2012).
7. M. Antkowiak, Y. Arita, K. Dholakia, and F. Gunn-Moore, J. Biomed. Opt. **16**, 120508 (2011).
8. E. Lukianova-Hleb, Y. Hu, L. Latterini, L. Tarpani, S. Lee, R. A. Drezek, J. H. Hafner, and D. O. Lapotko, ACS Nano **4**, 2109 (2010).
9. D. Bartczak, O. L. Muskens, T. M. Millar, T. Sanchez-Elsner, and A. G. Kanaras, Nano Lett. **11**, 1358 (2011).
10. E. Boulais, R. Lachaine, and M. Meunier, Nano Lett. **12**, 4763 (2012).
11. T. H. Wu, T. Teslaa, M. A. Teitell, and P. Y. Chiou, Opt. Express **18**, 23153 (2010).
12. T. H. Wu, T. Teslaa, S. Kalim, C. T. French, S. Moghadam, R. Wall, J. F. Miller, O. N. Witte, M. A. Teitell, and P. Y. Chiou, Anal. Chem. **83**, 1321 (2011).
13. L. Novotny and B. Hecht, *Principles of Nano-Optics* (Cambridge University, 2006).
14. Y. Seol, A. E. Carpenter, and T. T. Perkins, Opt. Lett. **31**, 2429 (2006).
15. V. K. Pustovalov, A. S. Smetannikov, and V. P. Zharov, Laser Phys. Lett. **5**, 775 (2008).
16. M. Tsukakoshi, S. Kurata, Y. Nomiya, Y. Ikawa, and T. Kasuya, Appl. Phys. B **35**, 135 (1984).
17. M. Antkowiak, M. L. Torres-Mapa, D. J. Stevenson, K. Dholakia, and F. J. Gunn-Moore, Nat. Protoc. **8**, 1216 (2013).
18. M. Terakawa, M. Ogura, S. Sato, H. Wakisaka, H. Ashida, M. Uenoyama, Y. Masaki, and M. Obara, Opt. Lett. **29**, 1227 (2004).
19. S. Sato, T. Ando, and M. Obara, Opt. Lett. **36**, 4545 (2011).
20. Y. Tomita, M. Tsubota, and N. An-Naka, J. Appl. Phys. **93**, 3039 (2003).